Environmental Engineering and Management Journal

March 2018, Vol. 17, No. 3, 631-640
http://www.eemj.icpm.tuiasi.ro/; http://www.eemj.eu

"Gheorghe Asachi" Technical University of Iasi, Romania

AN IMPROVED MODELING FOR PREDICTION OF PM2.5 COLLECTION EFFICIENCY IN ELECTROSTATIC PRECIPITATORS

Jian-Ping Zhang[1,2*], Zhen Gong[1], Jiong-Lei Wu[1], Helen Wu[3], Wei-Guo Pan[1]

[1]College of Energy and Mechanical Engineering, Shanghai University of Electric Power, Shanghai 200090, China
[2]Shanghai Key Laboratory of Materials Protection and Advanced Materials in Electric Power, Shanghai 200090, China
[3]School of Computing, Engineering and Mathematics, Western Sydney University, Sydney 2751, Australia

Abstract

In this work, PM2.5 removal mechanism was explored to investigate PM2.5 collection efficiency under the influences of applied magnetic field and diffusion charging (the main charging mode for submicron particle). The proposed electrostatic precipitators (ESPs) mathematical model considered three-field interaction between fluid field, electromagnetic field and particle dynamic field. CFD software FLUENT was used to generate the simplified solid structure of the ESP. In numerical calculation, the mathematical expressions for charge of dusty particles, drag force, electric force and Lorentz force were and input by using UDF. Deutsch-Anderson formula was applied to process and analyze CFD numerical solution to obtain the grade efficiency and overall efficiency of PM2.5. The results indicate that the PM2.5 grade efficiency increases non-linearly with increasing particle diameter when only applied magnetic field is considered. Both grade and overall efficiencies of PM2.5 improve under a strong magnetic field. The effect of magnetic field on collection efficiency also depends on the particle removal mechanisms. The PM2.5 grade efficiency under diffusion charging decreases first and then levels off. Furthermore, diffusion charging increases PM2.5 removal performance with the decrease of working potential or the increase of gas velocity. The diffusion charging mainly influences the fine particles in PM2.5 diameter range and is a much more important particle removal mechanism than magnetic field. Under the combined effect, the PM2.5 grade and overall efficiencies also increase with increasing magnetic field intensity, and dust removal ability of a wire-pipe ESP can be further improved in the entire PM2.5 diameter range.

Key words: applied magnetic field, diffusion charging, grade efficiency, multi-field coupling, overall efficiency, wire-pipe ESP

Received: August, 2013; Revised final: June, 2014; Accepted: June, 2014; Published in final edited form: February 2018

1. Introduction

Environmental protection has gained more and more attentions globally. The control of fine particulate pollutants, particularly whose aerodynamic equivalent diameter is less than 2.5 μm (PM2.5), has become the focus of many recent investigations (Falaguasta et al., 2008). The electrostatic precipitators (ESPs) presently used in power plants has high collection efficiency for particulate pollutants, whose aerodynamic equivalent diameter is more than 10 μm, and this collection efficiency can reach 99% (Wang et al., 2007; Zhang et al., 2016). However, for smaller particles like PM2.5, high collection performance still remains a challenge (Hu et al., 2017). Therefore, further research is needed in the field of removal mechanism exploration and ESP innovation design.

Recently, some researches on test method and numerical simulation have been done for fine particle removal in electrostatic precipitators ESPs (Falaguasta et al., 2008; Farnoosh et al., 2011; Hamou et al., 2017; Zhu et al., 2012). Falaguasta et al. (2008) investigated the PM2.5 collection efficiency of a laboratory-scale-plate-wire ESP by changing applied potential, gas velocity, diameter of the discharge electrode, the distance between electrodes, and the total precipitator length. Zhu et al. (2012) studied grade efficiency of

* Author to whom all correspondence should be addressed: e-mail: jpzhanglzu@163.com; Phone: +86-21-35303752; Fax: +86-21-35303752

fine particles in industrial electrostatic precipitators. They compared the corona current and the grade efficiency in an ESP with single-phase TR with those with three-phase TR. Farnoosh et al. (2011) used 3-D hybrid Finite Element (FE)–Flux Corrected Transport (FCT) numerical algorithm to evaluate electrical characteristics of a laboratory-scale-single-stage-spike-plate electrostatic precipitator and predict the collection efficiency of particles. Zhao et al. (2008) promoted a stochastic method to solve the population balance equation, and used the method of event-driven constant volume to simulate the collection process of particles with small size (such as PM2.5) in a small-scale single-stage wire-plate ESP. The agreement among the results of the Monte Carlo method, the experimental data and the results of method of moments is good. Gutiérrez Ortiz et al. (2010, 2011) focused towards dimensional analysis in ESP model building, showing both the reduction in effort and more effective modeling that can result. The predicted values of micron-sized particle removal efficiency given by models agree well with the experimental data. Yu et al. (2012) introduced an electro-coagulation dual-zone dust removal technology, combined with the characteristics of an automobile exhaust. They used multi-physics coupling software Comsol to establish the model of the automobile exhaust, and studied the collection efficiency of PM2.5 particles emitted by automobile exhaust by tracking the trajectories of the particles.

There are currently two active research areas for micron particle removal: one is the full consideration of the particle diffusion charging, and the other is the application of the magnetic effect. Long et al. (2010) employed nine different particle charging models to simulate particle dynamics in an ESP and compared the results with those published previously. They found that the lawless model considering both field charging and diffusion charging was the optimal option. Zhang et al. (2016) studied the influence of diffusion charging on PM10 collection efficiency by using numerical simulation. Moon et al. (1999) investigated the discharge, and SO_2 and CO gas removal characteristics in a wire-to-cylinder-type non-thermal plasma reactor under a crossed DC magnetic field. Zhang et al. (2011) described a strongly-coupled calculation procedure for the particle dynamics in ESPs subjected to the applied magnetic field only. They also performed a numerical analysis of the PM100 trajectories and the collection efficiency. As it is known, the applied magnetic field in an ESP can control the PM2.5 trajectories effectively and hence can improve the collection efficiency. The simultaneous influence of applied magnetic field and diffusion charging on particle collection has not yet been studied deeply. In this work, the removal mechanisms of diffusion charging and magnetic field under multi-field coupling between fluid, electromagnetic and particle dynamic fields are investigated. Solid modeling of a wire-pipe ESP and numerical simulation of PM2.5 removal performance under the combined effect are achieved (Bischof et al., 2007). Present results lay a significant foundation for optimal design of future innovative ESPs.

2. PM2.5 removal mechanisms

2.1. Diffusion charging

Diffusion charging is the electrized action of particles entering an ESP and then colliding with the negative ions and electrons in the irregular thermal motion (Cui, 1998). The key effect of diffusion charging on removal process of PM2.5 particles inside an ESP is more significant than that of field charging (Sun and Zhao, 1990). The field charging process of a particle inside an ESP completes as soon as it enters the electric field and its saturated charge is reached (Oglesby and Nichols, 1978). However, diffusion charging process continues as long as the thermal motion of negative ions and electrons does not stop, and the process ends only until a particle is collected or escapes from the electric field. The influence of diffusion charging on fine particles is larger than that of field charging and becomes more and more significant with decreasing particle size.

2.2. Applied magnetic field

Fig. 1 gives the schematic diagram of removal mechanism inside a wire-pipe ESP subjected to applied magnetic field. A wire-pipe ESP contains a discharge electrode wire and a grounding cylindrical collection electrode. The vertical section passing through the axis of the ESP can be simplified as a 2-D structure, and the direction of applied magnetic field is perpendicular to the electric field and the paper plane.

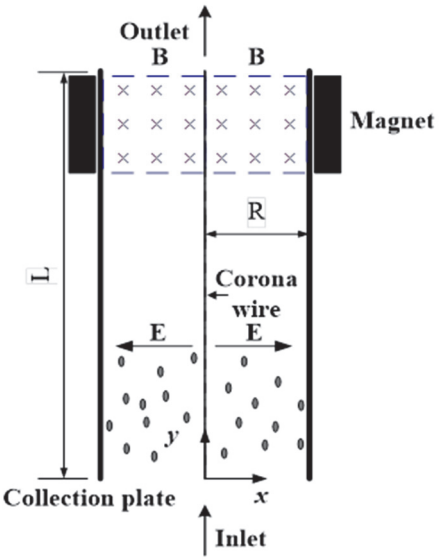

Fig. 1. Schematic diagram of removal mechanism inside a wire-pipe ESP under applied magnetic field

Application of magnetic field deflects the free electrons, and extends the travel distance between electrodes, increasing the possibility for contact and collision between free electrons, ions and dust

particles. PM2.5 particles can be charged more easily under the magnetic field than without it. Furthermore, PM2.5 particles move spirally under the combined action of Lorentz force and electric force (Yuan et al., 2001). They bend more and more towards collection electrode. Generally, the contact time between particle and collection electrode is prolonged, which improves the collection efficiency.

3. Mathematical model

3.1. Multi-field coupling relationship

Fluid field, electromagnetic field and particle dynamic field coexist and interact with each other inside an ESP. The specific coupling relationship is illustrated in Fig. 2.

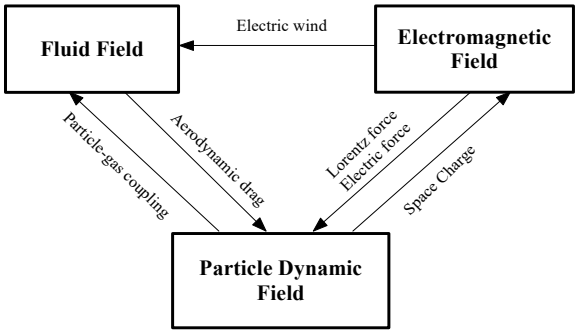

Fig. 2. Schematic diagram of multi-field coupling inside an ESP

3.2. Fluid field

The density of flue gas can be treated as a constant, assuming it is incompressible in a 2-D ESP model. The generalized source term is substituted by the sum of the aerodynamic drag and the electric body force in Navier-Stokes equations (Choi and Fletcher, 1997; Skodras et al., 2006). Hence, the mass conservation equation and momentum conservation equations can be expressed as (Eqs. 1-3):

$$\frac{\partial u_g}{\partial x}+\frac{\partial w_g}{\partial y}=0 \tag{1}$$

$$\frac{\partial(\rho_g u_g)}{\partial t}+\frac{\partial(\rho_g u_g u_g)}{\partial x}+\frac{\partial(\rho_g u_g w_g)}{\partial y}= =-\frac{\partial P}{\partial x}+(\mu+\mu_t)\left(\frac{\partial^2 u_g}{\partial x^2}+\frac{\partial^2 u_g}{\partial y^2}\right)+F_{Dx}+\rho E_x \tag{2}$$

$$\frac{\partial(\rho_g w_g)}{\partial t}+\frac{\partial(\rho_g u_g w_g)}{\partial x}+\frac{\partial(\rho_g w_g w_g)}{\partial y}= =-\frac{\partial P}{\partial y}+(\mu+\mu_t)\left(\frac{\partial^2 w_g}{\partial x^2}+\frac{\partial^2 w_g}{\partial y^2}\right)+F_{Dy}+\rho E_y \tag{3}$$

where ρ_g is the air density, in *kg·m*$^{-3}$; u_g and w_g are x and y velocity component of gas, respectively, in *m·s*$^{-1}$; P is the average static pressure of gas, in *Pa*; F_D is the aerodynamic drag force, in *N*; E_x and E_y are electric field strength, in *V/m*; x and y denote the directions parallel and perpendicular to the collection electrode of the 2-D ESP calculation region, respectively; ρ is the space-charge density, in *C/m*^{3}; μ is molecular dynamic viscosity of gas, in *kg/(m·s)*; μ_t is turbulent dynamic viscosity of gas, in *kg/(m·s)*, which can be expressed by the function of two arguments k and ε using the concept of eddy viscosity proposed by Boussinesq (Zhang et al., 2011), namely, $\mu_t=\rho_g C_\mu \frac{k^2}{\varepsilon}$; $C_\mu=0.09$ is an empirical constant.

3.3. Electromagnetic field

The calculation of electric field in a wire-pipe ESP can be simplified as a 1-D model (x direction) due to axial symmetry and neglect of end effect (Oglesby and Nichols, 1978). When space-charge of ions and charged particles exists in the electric field, the Poisson equation for electric potential, in coordinates in Fig. 1 can be written as (Eq. 4):

$$\frac{d^2U}{dx^2}+\frac{1}{x}\frac{dU}{dx}+\frac{\rho}{\varepsilon_0}=0 \tag{4}$$

where ε_0 is the permittivity of free space, in 8.854×10^{-12} *F/m*; x is the radial distance from a space point to the corona wire, in *m*; U is the potential, in *V*. ρ can be obtained using the relationship between current density J and electric field strength E at the location x apart from the corona wire, that is (Eq. 5):

$$\rho=\frac{J}{b_{eff}E} \tag{5}$$

where b_{eff} is the effective mobility of multiple space-charge carriers, which contains the ion space-charge mobility b_{ion}=*2.2·10*$^{-4}$ *m*^{2}*/(V×s)* and particle space-charge mobility b_{pc}=*5·10*$^{-7}$ *m*^{2}*/(V×s)*. As b_{pc} is very small and can be neglected. Thus, b_{eff} is calculated using the ion space-charge mobility only.

Substituting Eq. (5) into Eq. (4), and combining with the current density $J=\frac{I}{2\pi x}$ and the electric field strength $E=-\frac{dU}{dx}$, one can get (Eq. 6):

$$E\frac{dE}{dx}+\frac{E^2}{x}-\frac{I}{2\pi x\varepsilon_0 b_{eff}}=0 \tag{6}$$

where I being the current per unit of corona wire in *A/m*, can be expressed as (Xiang, 2002) (Eq. 7)

$$I=\frac{8\pi\varepsilon_0 b_{eff}}{R^2\ln(R/r_w)}U_0(U_0-U_C) \tag{7}$$

where R is the inner radius of pipe-like collection electrode in m; r_w is the radius of corona wire in m; U_o is the working voltage in V; U_C being the critical voltage in V, can be written as (Eq. 8)

$$U_C = r_w E_C \ln(R / r_w) \tag{8}$$

where E_C is the critical electric field strength (Xiang, 2002) in V/m.

Solving differential Eq. (6), we have (Eq. 9):

$$E = -\sqrt{\frac{I}{2p b_{eff} e_0} + \frac{\overline{C}^2}{x^2}} \tag{9}$$

where $\overline{C}$ is the integration constant, which can be obtained using the following expression (Eq. 10)

$$\overline{C} = \sqrt{r_w^2 (E_C^2 - \frac{I}{2p e_0 b_{eff}})} \tag{10}$$

It should be noted that the size and direction of the applied magnetic field B in the ESP is constant in this work, which means that the magnetic field doesn't change with either time or space.

3.4. Particle dynamic field

Particle dynamic field can be solved numerically by means of the integration of dynamic balance equation acting on particles in a 2-D plane. The inertial force equals the sum of forces acting on particles, and hence the equations of particle dynamic field can be written as (Eqs. 11 - 12):

$$m_p \frac{du_p}{dt} = Q_p u_p B + Q_p E_x + F_{D,x} \tag{11}$$

$$m_p \frac{dw_p}{dt} = Q_p w_p B + F_{D,y} \tag{12}$$

where m_p is the particle mass in kg; u_p and w_p denote the particle velocities in x and y directions, respectively, in m/s; Q_p is the total particle charge in C, and includes saturated charge due to field charging Q_{sat} and particle charge due to diffusion charging Q_{diff} (2011); $Q_p u_p B$ and $Q_p w_p B$ are the Lorentz forces acting on the moving charged particles, in N; $Q_p E_x$ is the electric force, in N; $F_D = m_p F_d$ and the drag force F_d for per unit mass of a single particle can be expressed as (Eq. 13):

$$F_d = \frac{1}{2} A_p \rho_g C_D \left(\overline{u}_g - \overline{u}_p\right) \left|\overline{u}_g - \overline{u}_p\right| \tag{13}$$

where A_p is the area of the particle facing flow direction, *in* m^2; $A_p = \pi D_i^2 / 4$, in m^2; D_i is the particle diameter, in m; $\overline{u}_g$ and $\overline{u}_p$ are the average velocity of flue gas and the particle, respectively, in m/s; C_D is the drag coefficient between flue gas and the particle.

It is necessary to point out that electric field distribution, calculated using analytical Eq. (9) acts on particle dynamic field by the second term on the right side of Eq. (11). The Lorentz force, generated by applied magnetic field also affects the particle dynamic field by means of two first terms on the right side of Eqs. (11) and (12). The coupling between particle dynamic field and fluid field is achieved by means of the aerodynamic drag force F_D.

3.5. Calculation of collection efficiency

After the numerical solution of particle dynamic field is obtained, Deutsch-Anderson semi-empirical formula (Oglesby and Nichols, 1978) is employed to calculate the grade efficiency and the overall efficiency of PM2.5 in the ESP. The collection electrode is divided into $\overline{N}+1$ sections in length, and all particles are classified into 34 diameter groups. Therefore, the grade efficiency of PM2.5 in the $i-th$ diameter can be written as (Zhang, 2011) (Eq. 14):

$$\eta_i = \frac{\sum_j \eta_{i,j} M_{i,j}}{M_{i,1}} \tag{14}$$

where $\eta_{i,j}$ is the collection efficiency of the particles with diameter D_i in the *j-th* section; $M_{i,j}$ is the particle concentration of *i-th* diameter in the *j-th* collection section area, and $M_{i,1}(j=1)$ denotes the $M_{i,j}$ at the inlet.

The overall efficiency η of PM2.5 in the wire-pipe ESP can be obtained using the following expression (Eq. 15):

$$\eta = \sum_i \eta_i P_i \tag{15}$$

where P_i is the mass flow rate of the particles with the *i-th* diameter at the inlet of the ESP.

4. CFD Model description

4.1. Simplified model and grid discretization

The simplified model of a wire-pipe ESP is shown in Fig. 1. The geometric parameters of the model are given as follows: the height of collection electrode $L=7.6\ m$; the radius of corona wire $r_w=1.0mm$; the distance between the outer surface of corona wire and the inner surface of collection electrode is approximated as the inner radius R of the pipe-like collection electrode, that is, $R = 0.3m$. The wire-pipe ESP is symmetric with respect to the axial line, and hence the section in the right side of the axis is selected as the calculation region. CFD pre-process software GAMBIT is used to discrete the region and generate the mesh. After careful check of the grid, the calculated region is finally divided into

$60 \times 380 = 22800$ elements with a uniform grid density. The generated mesh is shown in Fig. 3.

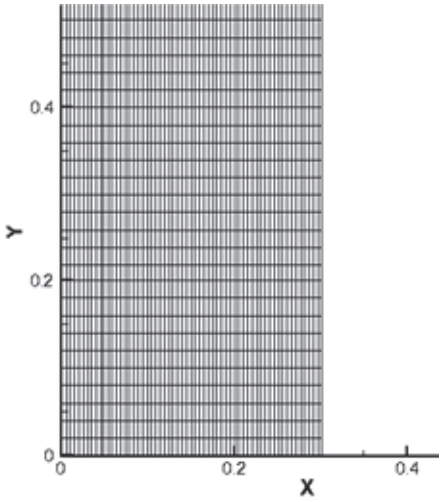

Fig. 3. Generated mesh in the calculated region of the wire-pipe ESP

4.2. Gas and solid phase parameters and boundary conditions

Gas and solid phase parameters should be obtained based on the real working conditions inside an ESP, and the correct selection of these parameters is a must for the reliability of the numerical simulation.

First of all, the properties of particles should be assumed. This study focuses on the inhalable PM2.5 particles emitted by coal plants. The particles are spherical and the volume fraction of particulate phase is usually less than 10%-12%. Therefore, the particles are treated as sparse particulate phase, and particle movement can be solved using DPM model. The physical properties of particles belong to anthracite. Material properties based on the flue gas data from coal plants are listed in Table 1. The diameter range of the particles is *[0.1 μm, 2.5 μm],* which satisfies Rosin-Rammler distribution, and the distribution parameters are: spread index *n=1.64* and mean diameter $D_{50}=0.5D_{max}$, $D_{max}=2.5\mu m$.

The gas phase in gas-solid two phase flow can be considered as a continuous medium. The flue gas, which almost doesn't react chemically with the dusty particles, can be simply treated as air, that is, the flue gas pressure is $P = 1.01 \times 10^5 Pa$. The flue gas at the inlet of the ESP is considered to be distributed evenly, and the velocity is completely vertical to the cross section of the entrance. The effect of corona wire on flue gas flow is neglected. At the given temperature $T_{ESP}=450K$, the gas density, constant-pressure specific heat, heat conductivity and dynamic viscosity of the flue gas are obtained by linear interpolation of property diagram (Yang and Tao, 2006).

Table 1. Physical parameters for inlet particles

Density (kg/m^3)	***Constant-pressure specific heat (J/Kg·K)***	***Thermal conductivity (W/m·K)***
2100	1680	0.0454

The physical parameters of the flue gas are given in Table 2. The boundary conditions of the wire-pipe ESP are presented in Table 3. T_i and D are the turbulence intensity and the equivalent diameter of the ESP inlet, respectively. Velocity inlet and pressure outlet are adopted as the corresponding boundary conditions for inlet and outlet of the flue gas. The potential of the corona wire surface is U_o, and the potential of collection electrode is set to be zero.

Standard law of wall is applied on the surface calculation of the collection electrode and corona wire, namely, a set of semi-empirical formulas (law of wall) are used to connect physical parameters of the wall to those in turbulent core region.

4.3. Numerical iterative process

After the equations are discretized by using FVM, the corrections to pressure, velocity and the nonlinear issue caused by multi-field coupling are made using the iterative method. The detailed iterative procedures are displayed in Fig. 4.

5. Results and discussions

5.1. Reliable verification of calculation

Numerical calculation in this part of the work was performed under the same wire-pipe ESP working conditions as those in the reference (Huang et al., 2007). Fig. 5 compares present overall efficiency with the result got by Huang et al. (2007). It is very clear that the calculated overall efficiency shows a very good agreement with the one in above-mentioned reference, and the relative error is less than 2%. The result indicates that the numerical model generated in this study can precisely simulate the particle collection efficiency in the ESP.

5.2. Influence of diffusion charging and magnetic fields on the particle trajectories

In order to observe more intuitively the removal effect in a wire-pipe ESP under the influences of diffusion charging and magnetic field, trajectories for different kinds of particles which follow the Rosin-Rammler distribution are simulated when $U_o=30kV$ and $v_o=0.5m/s$, as shown in Fig. 6.

Table 2. Physical parameters of the flue gas

Density (kg/m^3)	***Constant-pressure specific heat (J/kg·K)***	***Thermal conductivity (W/m·K)***	***Dynamic viscosity (kg/m·s)***
0.79	1090.33	0.038	2.39×10^{-5}

Table 3. Boundary Conditions of the wire-pipe ESP

	x-velocity	***y-velocity***	U	k	ε	***Particle***
Inlet	$u_g = 0$	$w_g = v_0$	$\nabla U = 0$	$3T_i^2 u_i^2 / 2$	$0.05k^{1.5}D$	Escape
Outlet	Pressure	Pressure	$\nabla U = 0$	$\partial k / \partial x = 0$	$\partial \varepsilon / \partial x = 0$	Escape
Corona wire	No slip	No slip	$U = U_0$	wall-function	wall-function	Reflect
Collection plate	No slip	No slip	$U = 0$	wall-function	wall-function	Trap

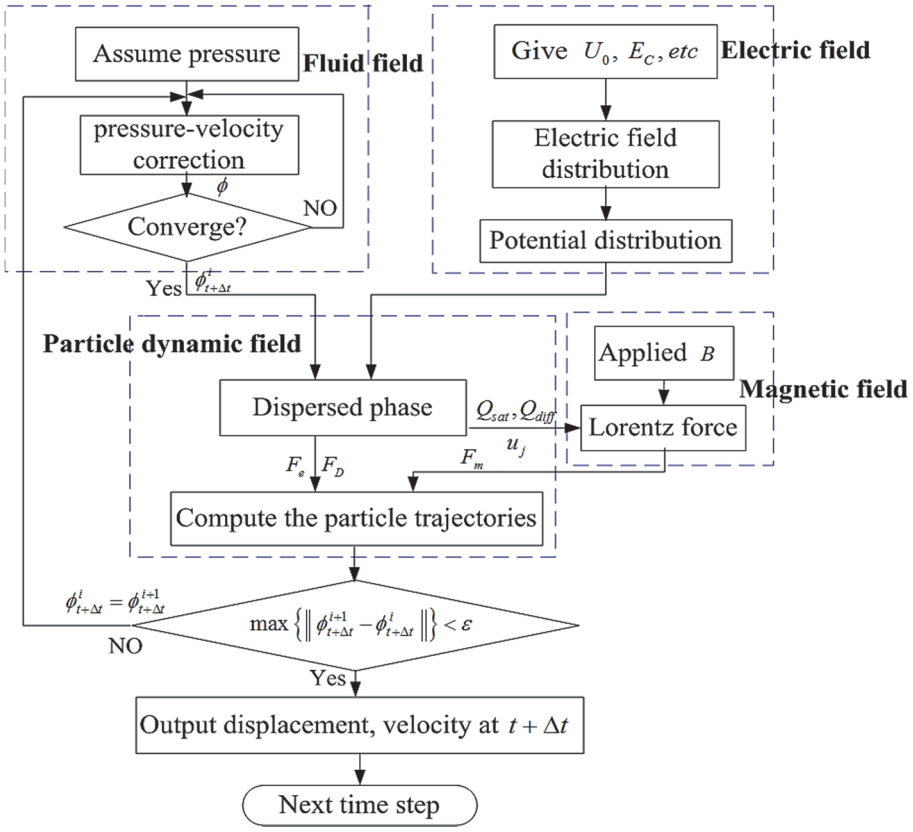

Fig. 4. Calculation flowchart for the ESP simulation

Figs. 6(a) and 6(b) respectively show the particle trajectories without and with diffusion charging. Fig. 6 (c) and (d) respectively exhibit the particle trajectories at *B=0.5T* and *B=1.0T* with diffusion charging considered.

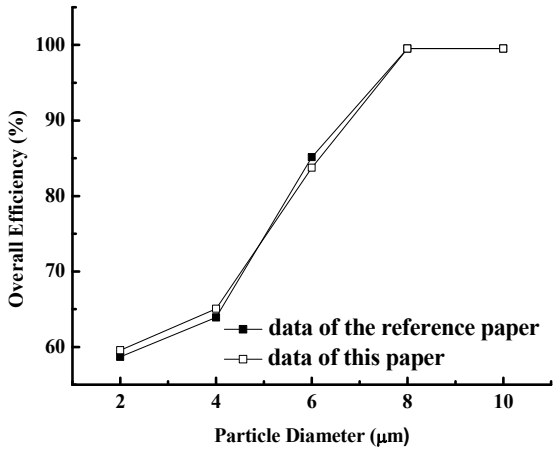

Fig. 5. Comparison of reference data with present results (v_0=*0.5 m/s*, U_0=*60 kV*)

Comparing Fig. 6(a) and (b), the particle trajectory shift is much more apparent in the direction of the dust collecting duct under the condition of diffusion charging, which means that diffusion charging cannot be ignored in the process of numerical simulation. As shown in Figs. 6 (b), 6(c) and 6(d), the particle trajectory bends more and more towards the collecting duct with the increase of the magnetic field, which implies that magnetic field can improve the removal efficiency.

5.3. Influence of diffusion charging on PM2.5 collection

Grade efficiency under different charging mechanisms is plotted in Fig. 7 to evaluate the specific influence of diffusion charging on PM2.5 collection in the ESP. PM2.5 grade efficiency with field charging alone shows a non-linear increase with increasing particle diameter, while it decreases first and then tends to be stable when diffusion charging is considered simultaneously. The difference in grade efficiency between two different charging

mechanisms represents the contribution due to diffusion charging. It can be seen that this contribution becomes greater with the decrease of particle diameter, as the effect of diffusion charging on fine particles is more obvious than that of field charging.

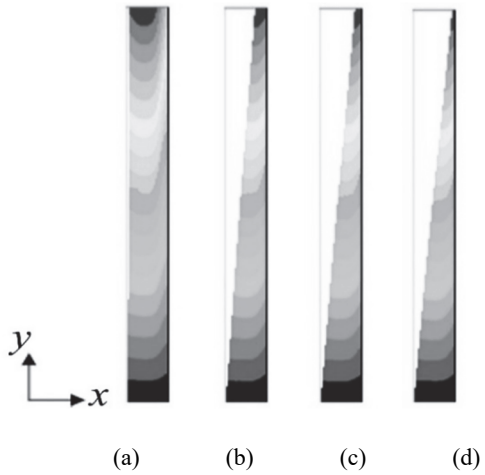

Fig. 6. Particle tracks in a wire-pipe ESP (v_0=0.5 m/s, U_0=30 kV)

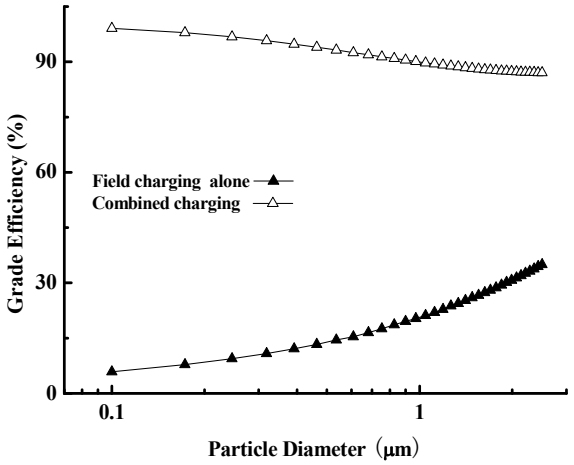

Fig. 7. PM2.5 grade efficiency under field charging alone and combined charging of field charging and diffusion charging (v_0=0.5 m/s, U_0=75 kV)

Fig. 8 shows PM2.5 overall efficiency as a function of working voltage inside the wire-pipe ESP with different gas velocities and charging mechanisms. At a given gas velocity, overall efficiency with field charging alone increases linearly with working voltage, while the one with combined charging shows a non-linear increase. The ratio of the difference in overall efficiency between two charging mechanisms to the overall efficiency with combined charging represents the percentage contribution of diffusion charging and is here denoted as the contribution rate c_0. It can be seen in Fig. 9 that the c_0 decreases almost linearly with working voltage, which indicates that the contribution of diffusion charging to PM2.5 collection efficiency is greater under the low-voltage condition. Furthermore, it is identified that the contribution of diffusion charging is also greater under the high-gas-velocity condition.

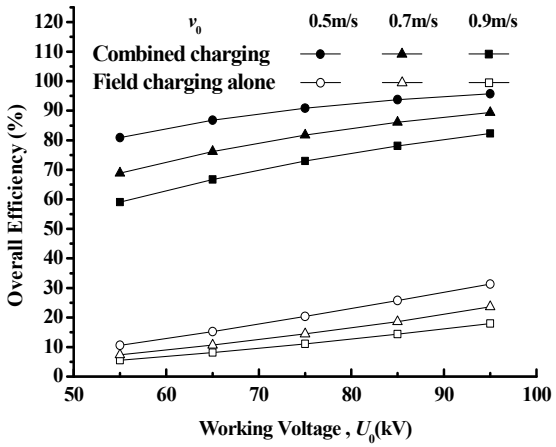

Fig. 8. PM2.5 overall efficiency versus working voltage with different gas velocities and charging mechanisms

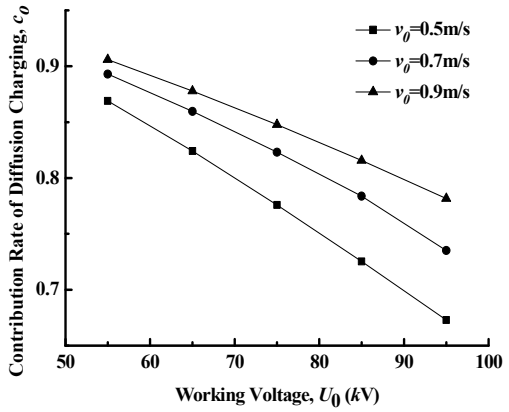

Fig. 9. The contribution rate c_0 as a function of working voltages under different gas velocities

5.4. Influence of applied magnetic field on PM2.5 collection

Fig. 10 exhibits the influence of applied magnetic field on PM2.5 collection efficiency. It is evident that the PM2.5 grade efficiency increases exponentially with increasing particle diameter, showing that the effect of magnetic field intensity depends strongly on the particle size and becomes greater for larger particles.

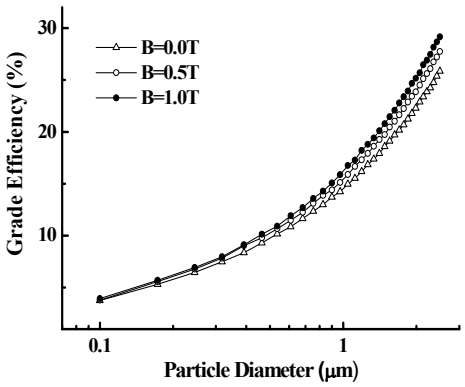

Fig. 10. PM2.5 grade efficiency versus particle diameter under different applied magnetic field intensities (v_0=0.7 m/s, U_0=75 kV)

Two effects of applied magnetic field on PM2.5 collection efficiency can be further identified in Fig. 10. Firstly, three curves become distinguishable with increasing particle diameter. Secondly, at a large particle diameter, the difference between middle curve and bottom one is larger than that between top curve and middle one, indicating that the increment in grade efficiency during a unit increment of magnetic field intensity decreases with increasing magnetic field intensity.

Fig. 11 presents the PM2.5 overall efficiency under the same conditions as used in Fig. 10. It is clear that PM2.5 overall efficiency of the wire-pipe ESP also increases with increasing magnetic field intensity. Fig. 11 also shows that the difference between middle bar and far left one is slightly larger than that between far-right bar and middle one, which is consistent with the second point drawn from Fig. 10.

5.5. Influence of combined effects on PM2.5 collection

PM2.5 grade efficiency under diffusion charging effect only, applied magnetic field effect only and combined effect is shown in Fig. 12. It can be seen that diffusion charging produces a much larger grade efficiency than applied magnetic field, particularly at small particle diameter. The PM2.5 grade efficiency with combined effect is higher than that with either diffusion charging only or applied magnetic field only. Obviously, combined effect can further improve PM2.5 grade efficiency, particularly for those coarse particles.

Further, from top four curves in Fig. 12, it can be seen, at a given particle size that the difference between two neighboring curves increases first and then decreases with increasing applied magnetic field intensity. Continuous increase of magnetic field intensity may come at a price. However, it is of great practical value to apply magnetic field to improve the removal ability of a wire-pipe ESP for those coarse particles in the PM2.5 range.

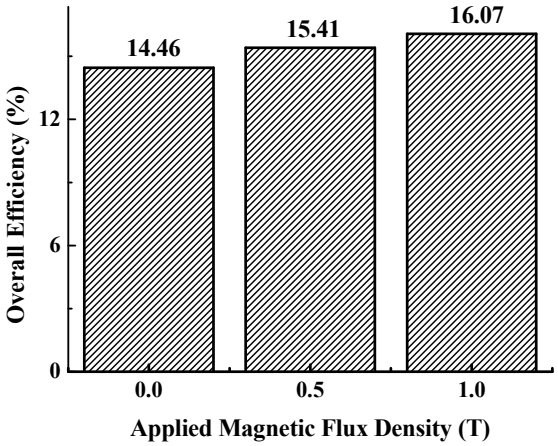

Fig. 11. PM2.5 overall efficiency under different applied magnetic fields in the wire-pipe ESP

Fig. 13 shows the overall efficiency as a function of magnetic field intensity under combined effect, noting that working conditions in Fig. 13 are the same as those in Fig. 12. It is clearly indicated that the overall efficiency of PM2.5 in the wire-pipe ESP also increases with the increase of magnetic field intensity. Further, the overall efficiency increment between two neighboring points becomes larger and then smaller with increasing magnetic field intensity. This overall efficiency increment at three equal intervals of magnetic field intensity is presented in Fig. 14 for a better viewing. It should be emphasized that this change of the increment with magnetic field intensity under combined effect is opposite to the change under magnetic field effect alone (Section 5.4), where the increment in either grade efficiency or overall efficiency from 0.5T to 1.0T is smaller than that from 0T to 0.5T (Figs. 10, 11).

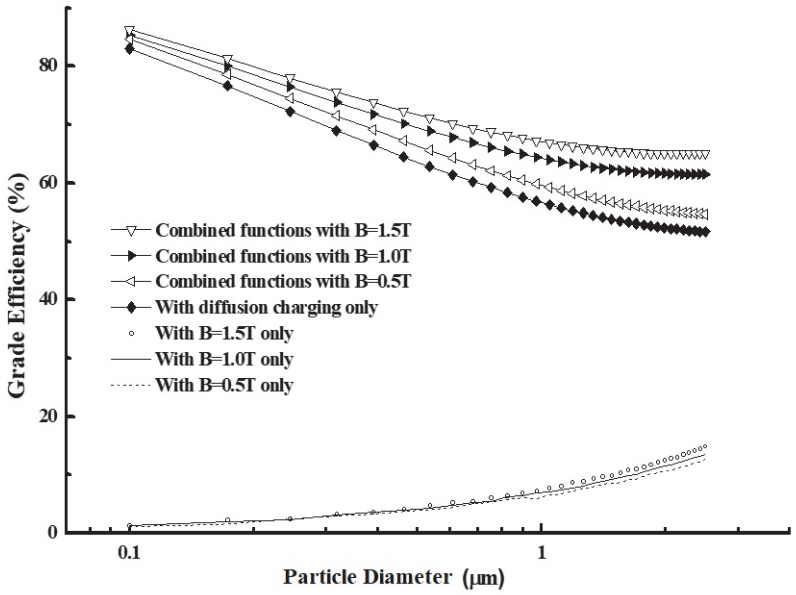

Fig. 12. PM2.5 grade efficiency versus particle diameter under different working conditions (v_o=*0.9 m/s,* U_o=*55kV*)

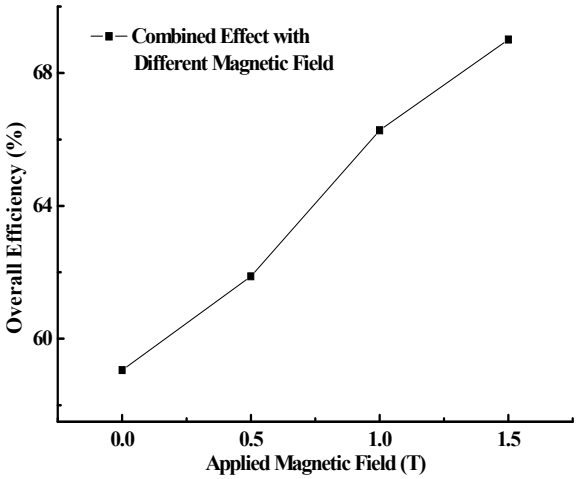

Fig. 13. PM2.5 overall efficiency versus applied magnetic field intensity under combined effect

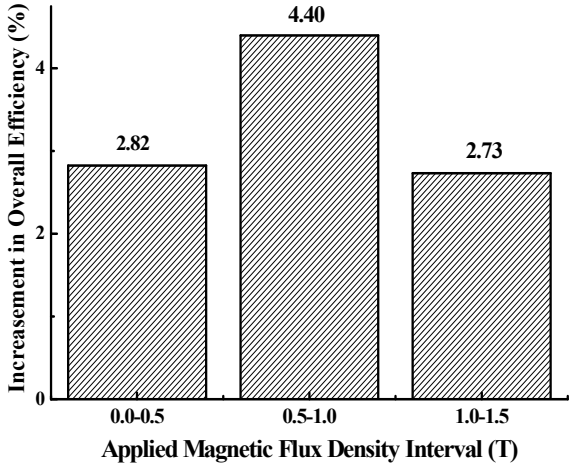

Fig. 14. The increment in PM2.5 overall efficiency at three equal intervals of magnetic field intensity under combined effect

The result indicates that the effect of magnetic field on collection efficiency also depends on the particle removal mechanism.

6. Conclusions

The mathematical model of a 2-D wire-pipe ESP under multi-field coupling was developed, and the PM2.5 removal mechanisms of diffusion charging and applied magnetic field were investigated. The PM2.5 collection efficiency was calculated and discussed in detail. The conclusions can be drawn as follows:

(1) The variation of the PM2.5 grade efficiency with particle diameter shows different behaviors with or without diffusion charging. Diffusion charging has dominant effects on fine particles in PM2.5 range and improves the dust collection efficiency of the ESP significantly, in particularly at the low working voltage or high gas velocity.

(2) The PM2.5 grade and overall efficiencies increase with the increase of the applied magnetic field intensity, indicating the positive contribution of the magnetic field. It was also identified that the use of magnetic field is more effective for the coarse particles in the PM2.5 particle range. Further, it was found that the effect of magnetic field on collection efficiency also depends on the particle removal mechanism.

(3) The effect of diffusion charging on PM2.5 removal is greater than that of magnetic field, which becomes more obvious with decreasing particle diameter. PM2.5 removal performance with combined effects is better than that with either diffusion charging only or applied magnetic field only. The results provide engineers with important technical information for the ESP optimal design and collection efficiency prediction.

Acknowledgments

This work is supported by the Program of National Natural Science Foundation of China (11572187); Foundation of Science and Technology Commission of Shanghai Municipality (15110501000, 14DZ2261000, 11DZ2281700).

References

Bischof C.H., Bucker H.M., Rasch A., Slusanschi E., Lang B., (2007), Automatic differentiation of the general-purpose computational fluid dynamics package FLUENT, *Journal of Fluids Engineering*, **129**, 652-658.

Choi B.S., Fletcher C.A.J., (1997), Computation of particle transport in an electrostatic precipitator, *Journal of Electrostatics*, **40-41**, 413-430.

Cui B.X., (1998), Charging theory on powder particulates in electrostatic corona field, *Yantai Teachers College Journal (Natural Science)*, **14**, 106-109.

Falaguasta M.C.R., Steffens J., Valdes E.E., Coury J.R., (2008), Overall collection efficiency of a plate-wire electrostatic precipitator operating on the removal of PM2.5, *Latin American Applied Research*, **38**, 179-186.

Farnoosh N., Adamiak K., Castle G.S.P., (2011), Numerical calculation of submicron particle removal in a spike-plate electrostatic precipitator, *IEEE Transactions on Dielectrics and Electrical Insulation*, **18**, 1439-1452.

Gutiérrez Ortiz F.J., Navarrete B., Cañadas L., (2010), Dimensional analysis for assessing the performance of electrostatic precipitators, *Fuel Processing Technology,* **91**, 1783-1793.

Gutiérrez Ortiz F.J., Navarrete B., Cañadas L., (2011), Assessment of plate–wire electrostatic precipitators based on dimensional and similarity analyses, *Fuel*, **90**, 2827-2835.

Hamou N., Massinissa A., Hakim A., Youcef Z., (2017), Active electrode shape effect on the corona discharge in an electrostatic precipitator, *Environmental Engineering and Management Journal,* **16**, 2545-2551.

Hu B., Zhang L., Yi Y., Luo F., Liang C., Yang L.J., (2017), PM2.5 and SO_3 collaborative removal in electrostatic precipitator, *Powder Technology*, **318**, 484-490.

Huang Z., Deng Q.H., Cai H.X., (2007), Performance research of wire pipe electrostatic precipitators, *Building Energy & Environment*, **26**, 95-98.

Long Z.W., Yao Q., (2010), Evaluation of various particle charging models for simulating particle dynamics in electrostatic precipitators, *Journal of Aerosol Science*, **41**, 702-718.

Moon J.D., Lee G.T., Chung S.H., (1999), SO_2 and CO gas removal and discharge characteristics of a nonthermal plasma reactor in a crossed DC magnetic field, *IEEE Transactions on Industry Applications*, **35**, 1198-1205.

Oglesby S., Nichols Jr G.B., (1978), *Electrostatic Precipitation*, Marcel Dekker, Inc., New York.

Skodras G., Kaidis S.P., Sofialidis D., Faltsid O., Grammelisc P., Sakellaropoulosa G.P., (2006), Particulate removal via electrostatic precipitators- CFD simulation, *Fuel Processing Technology*, **87**, 623-631.

Sun Q.M., Zhao H.Y., (1990), The electrification mechanism of particle on electrostatic precipitation, *Songliao Journal*, **4**, 48-51.

Wang P., Luo Z.Y., Xu F., Hou Q.H., Gao X., C.K.F., (2007), PM2.5 removal from coal-fired power plant with combined ESP and pulse charge pretreatment, *Acta Scientiae Circumstantiae*, **27**, 1789-1792.

Xiang X.D., (2002), *Modern Aerosol Particle Collection Theory and Technology*, Metallurgical Industry Press, Beijing, China.

Yang S.M., Tao W.X., (2006), *Heat Transfer*, Higher Education Press, Beijing, China.

Yu Z., Yang R., Liu H.Y., Xu L.W., (2012), Automobile exhaust PM2.5 simulation study of the electrostatic removal, *Hunan Agricultural Machinery*, **39**, 99-101.

Yuan N.W., Yang W., Lou J.Y., Rong M.Z., (2001), Research on the efficiency of air purification by collecting pre-charged suspend particles with the magnetic field, *Journal of Xi'an Jiaotong University*, **35**, 785-789.

Zhao H.B., Zheng C.G., (2008), A stochastic simulation for the collection process of fly ashes in single-stage electrostatic precipitators, *Fuel*, **87**, 2082-2089.

Zhang J.P., Ding Q.F., Dai Y.X., Ren J.X., (2011), Analysis of collection efficiency in wire-duct electrostatic precipitators subjected to the applied magnetic field, *IEEE Transactions on Plasma Science*, **39**, 569-575.

Zhang J.P., Zhang X., Shi F.F., Zha Z.T., Du Y.Y., Wu H., (2016), Diffusion charging effects on PM10 collection efficiency in a wire-pipe ESP under multi-field coupling, *Environmental Engineering and Management Journal*, **15**, 2367-2374.

Zhu J.B., Zhao Q.X., Yao Y.P., Luo S.K., Guo X.C., Zhang X.M., Zeng Y.X., Yan K.P., (2012), Effects of high-voltage power sources on fine particle collection efficiency with an industrial electrostatic precipitator, *Journal of Electrostatics*, **70**, 285-291.